A molecular dynamics simulation study of the pressure-volume-temperature behavior of polymers under high pressure

Justin B. Hooper,[1] Dmitry Bedrov,[1] Grant D. Smith,[1,a)] Ben Hanson,[1] Oleg Borodin,[2] Dana M. Dattelbaum,[3] and Edward M. Kober[3]
[1]*Department of Materials Science and Engineering, University of Utah, Salt Lake City, Utah 84112, USA*
[2]*Wasatch Molecular, Incorporated, 2141 E. St. Mary's Drive, Salt Lake City, Utah 84108, USA*
[3]*Los Alamos National Laboratory, Los Alamos, New Mexico 87545, USA*

(Received 14 November 2008; accepted 1 December 2008; published online 9 April 2009)

Isothermal compression of poly (dimethylsiloxane), 1,4-poly(butadiene), and a model Estane® (in both pure form and a nitroplasticized composition similar to PBX-9501 binder) at pressures up to 100 kbars has been studied using atomistic molecular dynamics (MD) simulations. Comparison of predicted compression, bulk modulus, and U_s-u_p behavior with experimental static and dynamic compression data available in the literature reveals good agreement between experiment and simulation, indicating that MD simulations utilizing simple quantum-chemistry-based potentials can be used to accurately predict the behavior of polymers at relatively high pressure. Despite their very different zero-pressure bulk moduli, the compression, modulus, and U_s-u_p behavior (including low-pressure curvature) for the three polymers could be reasonably described by the Tait equation of state (EOS) utilizing the universal *C* parameter. The Tait EOS was found to provide an excellent description of simulation *PVT* data when the *C* parameter was optimized for each polymer. The Tait EOS parameters, namely, the zero-pressure bulk modulus and the *C* parameter, were found to correlate well with free volume for these polymers as measured in simulations by a simple probe insertion algorithm. Of the polymers studied, PDMS was found to have the most free volume at low pressure, consistent with its lower ambient pressure bulk modulus and greater increase in modulus with increasing pressure (i.e., crush-up behavior). © *2009 American Institute of Physics*.
[DOI: 10.1063/1.3077868]

I. INTRODUCTION

Polymers and polymeric composites can be subjected to high pressures during processing and in their applications. The latter is particularly true for polymers in energetic materials applications, such as explosives, explosive devices, and propellants. For example, polymers constitute the major component of the binder phase in plastic bonded explosives, or PBXs. Understanding the pressure-volume-temperature (*PVT*) behavior of polymers under high pressure would be particularly valuable for deriving appropriate equation of state (EOS) and constitutive models for modeling and predicting the response of both the polymer and polymer composites to extreme conditions. Unfortunately, measuring the *PVT* behavior of amorphous materials at high pressure is difficult. Common techniques such as x-ray diffraction that take advantage of the crystalline structure of metals and ceramics are of limited value.[1] Static dilatometry measurements on polymers, where available, are typically limited to pressures below about 2 kbars. Diamond anvil measurements, while able to access higher pressure, appear to be plagued by difficulties in determination of compression (volume) for amorphous polymers, as illustrated below. Dynamic measurements, such as isentropic compression and shock (e.g., plate-impact) measurement, can provide useful data to high pressure but are difficult to perform to high pressures because of inherent low bulk sound speed in polymers.[1]

An alternative approach to experimental measurement of polymer properties at high pressure is to perform molecular dynamics (MD) simulations at elevated pressures. We have illustrated previously that MD simulations of polymers utilizing validated quantum-chemistry-based potentials can capture the properties of polymers at low pressures.[2] Furthermore, we have shown the MD simulations of crystalline energetic materials similarly utilizing accurate potentials capture the behavior of these materials to high pressures.[3,4] In this study, we investigate the ability of MD simulations utilizing validated potentials to capture compression of three polymers used as binders in PBX formulations, namely, poly(dimethylsiloxane) (PDMS), 1,4-polybutadiene (PBD), and a model of the poly(ester urethane) Estane® both with and without nitroplasticizers (model Estane and np-Estane, respectively), to high pressures.

II. SIMULATION METHODOLOGY

A. Polymer models

PDMS. MD simulations of PDMS were performed on an ensemble of ten chains of 19 repeat units each (1571 g/mol). A noncharged, nonpolarizable united atom (UA) force field, where each methyl group is treated as a single force center, was used. The UA repeat unit for PDMS is shown in Fig. 1(a). The force field has been parametrized to reproduce the

a)Electronic mail: gds8@utah.edu.

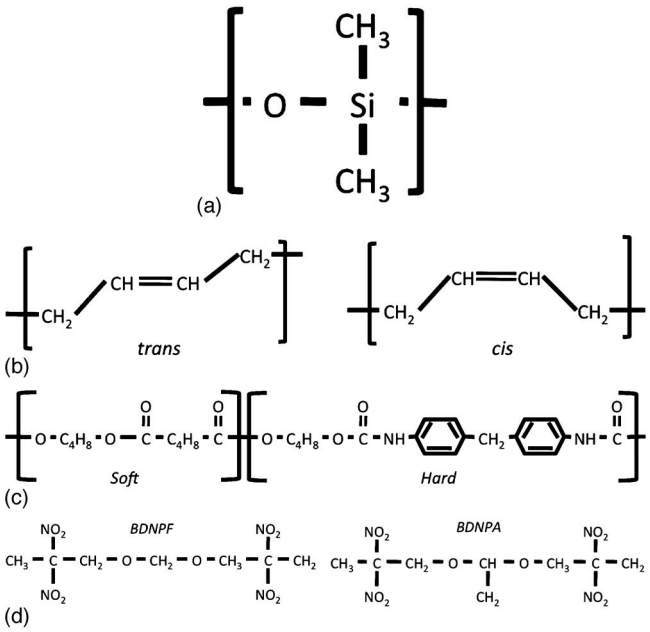

FIG. 1. Repeat units for (a) poly(dimethyl siloxane), (b) poly(butadiene), (c) and Estane®, as well as the structures of the nitroplasticizers (d) used in np-Estane simulations, BDNPF and bis(2,2-dinitropropyl) acetal. In (a) and (b), the carbons represent UA carbons, while (c) and (d) are fully atomistic representations.

density and heat of vaporization of PDMS oligomers analogously to our previous work in deriving an all atom PDMS force field.[5] The Si–C(H_3) bond length in the UA force field was increased from the value used in the fully atomistic force field to reflect the location of the center of mass of the –CH_3 group. Torsional parameters have been set to zero for the backbone dihedrals to prevent singularities arising from the linearization of the Si–O–Si bend. The Si–O–Si bend force constant and equilibrium angle in the UA force field were fitted to reproduce the angular distribution from MD simulations using our all atom force field.[5] The UA PDMS force field parameters are given in the supplemental information of this paper.[6]

PBD. The PBD system is described in detail in Ref. 7. Briefly, we generated an ensemble of 40 random copolymer chains each comprised of 30 units with a microstructure of 40% / 50% / 10% 1,4-*cis*/1,4-*trans*/1,2-*vinyl* units. These chains have a molecular weight of 1622 Da. The nonpolar UA force field for PBD is described in Ref. 7. The UA 1,4-*cis* and 1,4-*trans* repeat units for PBD are shown in Fig. 1(b). This PBD model and potential have been employed in numerous MD simulations of PBD melts,[7–16] including the pressure dependence of melt structure.[13]

Estane®. An ensemble of 14 copolymer chains of an Estane-like poly(ester urethane) oligomer forms the basis of our Estane® related simulations. The pure model Estane® system consists of only the poly(ester urethane) component of the system, while the nitroplasticized model (np-Estane) simulation is conducted with the addition of 56 molecules of bis(2,2-dinotropropyl)formal (BDNPF) and 54 molecules of bis(2,2-dinitropropyl)acetal (BDNPA), as described in Ref. 17. Each copolymer chain of model Estane® (2510 g/mol) had the structure $S_2H_2S_5H_1S_2$, where S represents a poly(butylene adipate) soft segment with one 1,4-butanediol (BDO) linkage and H represents a bis-1,1′-(methyl phenyl-4-isocyanate) (diphenyl-methane diisocyanate) unit with one BDO linkage as shown in Fig. 1(c). The nitroplasticizer molecules are illustrated in Fig. 1(d). The binder system so formed was a 1:1 mixture by weight of model Estane® and nitroplasticizer, the same ratio as in the binder in PBX-9501, and is labeled np-Estane. Previously developed quantum-chemistry-based atomistic force fields for Estane® (Ref. 18) and BDNPF/A nitroplasticizer[19] were used in the simulations.

B. Simulation details

The MD simulation package LUCRETIUS[20] employing the Nose–Hoover thermostat[21,22] and Anderson–Hoover barostat[22,23] was used for all simulations. All simulations were conducted at 298 K. Pressures ranging from ambient to over 100 kbars were investigated. Covalent bond lengths were constrained using the SHAKE algorithm.[24] Cutoff radii of 10, 11, and 9 Å were used for all van der Waals interactions for the Estane® based systems, PDMS, and PBD, respectively. In order to account for long-range electrostatic interactions in the np-Estane and model Estane® systems, the particle mesh Ewald (PME) algorithm[25] was used. The time step for the reciprocal part of PME calculations was 2 fs. A multiple time step reversible reference system propagator algorithm[26] was employed for integrating equations of motion for all polymers. The time step of integration for high frequency vibrations (bends and torsions) was 0.5 fs except for PBD where a 1 fs timestep was used. For the model and np-Estane simulations, nonbonded interactions within a cutoff radius of 6 Å were evaluated every 1 fs, while those between 6 and 10 Å were evaluated every 2 fs. For PDMS, nonbonded interactions within a cutoff radius of 6.5 Å were evaluated every 2 fs, while those between 6.5 and 11 Å were evaluated every 4 fs. For PBD, all nonbonded interactions were evaluated every 5 fs. During the MD simulations, the nonbonded interactions between atoms separated by two or less bonds were excluded, while full nonbonded interactions were included for atoms separated by three or more bonds.

All molecules were initially placed on a low-density cubic lattice with periodic boundary conditions at elevated temperatures. The cubic system was simulated for about 3 ns using *NPT* (constant number of particles, pressure, and temperature) ensemble while the volume was decreased to yield an average pressure of 1 atm. Equilibration for about 10 ns was conducted in the *NPT* ensemble at ambient pressure. The pressure was then increased to the next highest value and equilibration ranging from 10 to 50 ns was carried out. This process was repeated for all pressures. Production runs in the *NPT* ensemble were of 20 ns (np-Estane)–300 ns (PDMS) in duration.

C. Property determination and EOS models

1. EOS

The isothermal pressure-volume data from our MD simulations were fitted (see below) with the empirical Tait EOS:[27]

$$\frac{V(P)}{V_0} = 1 - C\ln\left(1 + \frac{P}{B}\right), \tag{1}$$

where P is pressure, V is volume, and V_0 is volume at zero pressure. The parameter B is a function of temperature and depends on the specific material. A "universal" value of C =0.089 36 has been found to work well for many polymer melts.[27,28]

2. Bulk modulus

The isothermal bulk modulus is defined as[29]

$$\kappa_T(P) = -V\left(\frac{\partial P}{\partial V}\right)_T. \tag{2}$$

The bulk modulus can be determined from *NPT* simulations at any pressure from volume fluctuations and is given as[30]

$$\kappa_T = \frac{k_B T\langle V\rangle}{\langle \delta V^2\rangle}, \tag{3}$$

where k_B is Boltzmann's constant, V is the instantaneous volume, and the brackets indicate an ensemble average. For the Tait EOS, κ_T is given by

$$\kappa_T = \left[1 - C\ln\left(1 + \frac{P}{B}\right)\right]\left[\frac{B+P}{C}\right], \tag{4}$$

which at zero pressure reduces to

$$\kappa_0 = \frac{B}{C}, \tag{5}$$

where κ_0 is the zero-pressure bulk modulus. Using Eq. (5), it is possible to recast Eqs. (1) and (4) as

$$\frac{V(P)}{V_0} = 1 - C\ln\left[1 + \left(\frac{P}{\kappa_0}\right)\Big/ C\right], \tag{6}$$

$$\frac{\kappa_T}{\kappa_0} = \left\{1 - C\ln\left[1 + \left(\frac{P}{\kappa_0}\right)\Big/ C\right]\right\}\left\{1 + \left(\frac{P}{\kappa_0}\right)\Big/ C\right\}, \tag{7}$$

respectively. We note that if a universal value of the parameter C is used, the Tait EOS predicts that all materials will show identical compression and pressure-dependent normalized (κ_T/κ_0) bulk modulus behavior when expressed as a function of normalized (P/κ_0) pressure.

3. Free volume

The free volume of the systems was calculated using a simple Monte Carlo insertion probe, where random coordinates are chosen for the center of a spherical probe of radius R_p, and that probe is checked for overlap with all atoms within the system. The atomic radii for the atoms of the system were taken as the distance at which the repulsion/dispersion energy with an identical atom was equal to k_BT at 298 K. For each system, a minimum of 10,000 different configurations (snapshots) was utilized, with a minimum time of 1 ps between each configuration. For each configuration, 500 independent insertion attempts were generated. A single insertion attempt consists of random generation of coordinates within the simulation box for the location of the spherical probe, followed by calculating the distance of the probe in relation to every force center within the box. If the distance between the two is less than the sum of the atom and probe radii, the probe is considered to have unsuccessfully sampled unoccupied space. The overall ratio of successful sampling of unoccupied space to total samplings is taken as the free volume fraction f_{fv} in the system. In order to properly calibrate the probe size, we utilized our PDMS system at 298 K and atmospheric pressure as the reference system and have calculated the respective probe size necessary to yield about 10% free volume as estimated for PDMS by combining the methods of Williams–Landel–Ferry and Doolittle,[1] yielding R_p=0.75 Å. This probe radius was utilized subsequently for all polymers and pressures.

4. Sound speed, shock speed, and particle velocity

The sound speed can be estimated from[31]

$$c_0 = (\kappa_0/\rho_0)^{1/2}. \tag{8}$$

The sound speed should be determined using the isentropic bulk modulus. However, for most materials the difference between the isothermal and isentropic modulus is small and we have therefore utilized Eq. (8). The shock speed U_s and particle velocity u_p are given by the Hugoniot jump conditions derived from conservation of mass, momentum, and energy as[31]

$$U_s = \left[\frac{P - P_0}{\rho_0}\frac{1}{1 - V/V_0}\right]^{1/2}, \tag{9}$$

$$u_p = U_s[1 - V/V_0]. \tag{10}$$

Equations (9) and (10) can be used to transform shock Hugoniot data (U_s and u_p) into the P-V plane along the shock Hugoniot. While Eqs. (9) and (10) hold strictly only for $P(V)$ along the shock Hugoniot, it is common to apply these relationships to $P(V)$ along an (typically ambient temperature) isotherm or an isentrope, yielding compression data in the "pseudo" U_s-u_p plane,[32] a transformation that neglects the effects of shock heating. In this paper, we will refer to U_s-u_p data shock measurements as well as transformation of isothermal and isentropic $P(V)$ data simply as U_s-u_p data. Similarly, $P(V)$ data will be referred to as compression data regardless of thermodynamic path (Hugoniot, isotherm, or isentrope). The thermodynamic conditions associated with each set of compression data (Hugoniot, isotherm, or isentrope) utilized in this paper are summarized in Table I.

For the Tait EOS, the normalized (by the speed of sound) shock and particle velocities can be expressed as

TABLE I. Summary of investigated polymers. Bolded values represent calculated quantities, while nonbolded represent reported data.

Source	Experiment	ρ_0 (g/cm^3)	K_0 (GPa)	c_0 (m/s)	P (GPa)	V (cm^3/g)	U_s (m/s)	U_p (m/s)	Other
				Sylgard® 184					
Datttelbaum *et al.*[a]	Optical diamond anvil cell	1.05	1.0–1.2 (Tait)	**976**	0.49–8.3[b]	0.952–0.608[b]	**976–480**	**0–1644**	
Stevens *et al.*[c]	Dilatometry	1.125	0.96 (Tait)[b]	**924**	0–0.200	0.889–0.800	**924–1382**	**0–133**	
Stevens *et al.*[c]	Brillouin diamond anvil cell	1.05	1.14	1319 **(1042)**	0.0–11.2	**0.952–0.498**	N/C	N/C	C_{11}, C_{12}, Poisson ratio
Marsh[d]	High explosive Hugoniot	1.037	⋯	⋯	0.75–15	0.788–0.525	2000–6000	350–2600	
				PDMS					
Sachdev *et al.*[e]	NOVA Swiss pressure chamber	0.956	0.84 (Tait)	**937**	0–0.26	1.05–0.922	**937–1488**	**0–180**	
Dattelbaum *et al.*[f]	Gas gun Hugoniot	⋯	⋯	⋯	0–8.67	⋯	947–4856	0–2047	
This work	UA MD simulation	0.950	1.05	1041	0–10.4	1.05–0.635	1041–5259	0–2086	
				np-Estane					
Gustavsen *et al.*[g]	Dilatometry	1.276	2.93	**1515**	0–0.20	0.784–0.743	**1502–1740**	**0–90.5**	
Gustavsen *et al.*[g]	Z-machine(Isentropic)	1.276	3.54[h]	**1665**	0–3.20	0.784–0.614	**1665–3405**	**0–736**	
Johnson *et al.*[i]	Gas gun Hugoniot	1.270	3.65	1690	**0.197–0.412**	**0.755–0.730**	1900–2200	80–160	
This work	EA MD Simulation	1.267	3.77	1709	0–5.06	0.789–0.586	1709–4815	0–1014	
				HTPB					
Gupta and Gupta[j]	Gas gun Hugoniot	⋯	⋯	⋯	0.1–0.8	Ratio only	⋯	⋯	
Barlow[k]	Dilatometry	0.897	⋯	⋯	0.0–0.243	1.12–1.02	**1366–1801**	**4.92–149**	
Millet *et al.* HTPB 1[l]	Gas gun Hugoniot	0.85	⋯	1460 (1530)[m]	**0.254–2.14**	**1.09–0.942**	1980–3550	150–710	
Millet *et al.* HTPB 2[l]	Gas gun Hugoniot	1.06	⋯	1430 (1650)[m]	**0.380–2.12**	**0.860–0.739**	2010–3040	180–660	
This Work	UA MD Simulation	0.915	1.41	1243	0–4.05	1.09–0.763	1243–3833	0–1155	
				Estane®					
Marsh[d]	High explosive Hugoniot	1.186	⋯	⋯	1.125–18.29	0.518–0.737	2609–6438	346–2395	
Johnson *et al.*[i]	Gas gun Hugoniot	1.190	3.69	1750	**0.191–0.952**	**0.810–0.751**	2110–2750	76–29	
Stevens *et al.*[c]	Dilatometry	1.183	3.25	**1657**	0.0–0.200	0.845–0.803	**1657–2037**	**0–102**	
Stevens *et al.*[c]	Brillouin diamond anvil cell	1.190	5.20	**2090**	0.0–12.27	0.781–0.551	**3308–5474**	**277–1883**	

TABLE I. (*Continued.*)

Source	Experiment	ρ_0 (g/cm^3)	K_0 (GPa)	c_0 (m/s)	P (GPa)	V (cm^3/g)	U_s (m/s)	U_p (m/s)	Other
This Work	EA MD simulation	1.177	4.22	1893	0–5.06	0.849–0.640	1893–4178	0–1030	

[a]Reference 1.
[b]Included in the reference's supplemental data.
[c]Reference 38.
[d]Reference 37.
[e]Reference 35.
[f]Reference 36.
[g]Reference 33.
[h]The indicated value is the singular instance of an isentropic bulk modulus within the data investigated. All other bulk modulus are isothermal.
[i]Reference 34.
[j]Reference 40.
[k]Reference 39.
[l]Reference 41.
[m]The value of c_0 fit from the linear Hugoniot EOS is significantly higher than that found when probing the longitudinal sound speed of the unpressurized polymer. The former is reported in parentheses.

$$\frac{U_s}{c_0} = \left\{ \frac{P}{\kappa_0} \frac{1}{C \ln\left[1 + \left(\frac{P}{\kappa_0}\right) \Big/ C\right]} \right\}^{1/2}, \tag{11}$$

$$\frac{U_p}{c_0} = \left\{ \frac{P}{\kappa_0} \frac{1}{C \ln\left[1 + \left(\frac{P}{\kappa_0}\right) \Big/ C\right]} \right\}^{1/2} C \times \ln\left[1 + \left(\frac{P}{\kappa_0}\right) \Big/ C\right], \tag{12}$$

assuming a reference pressure of zero. Hence, the normalized shock and particle velocity are predicted to be universal functions of the normalized pressure (which can be thought of simply as a parametric variable) assuming a universal value of the C parameter.

III. RESULTS AND DISCUSSION

A. Experimental data

Experimental data for the systems investigated represent a variety of measurement techniques, as summarized in Table I. For the four polymers investigated here, most of the experimental techniques utilized break down along the traditional boundaries depending on the desired pressures of investigation. At low pressures, dilatometry is used to generate isothermal compression curves up to approximately 2 kbars. For amorphous polymers at pressures higher than this, it is generally necessary to resort to shock propagation experiments that compress the polymer along the Hugoniot compression curve (with associated shock heating effects), rather than generate isothermal compression data. In addition to the more standard dilatometric and shock loading techniques, newer isentropic and isothermal loading techniques at higher pressures have been employed, as described below.

For np-Estane, Gustavsen *et al.* provided compression densities up to 2 kbars generated through dilatometry[33] but also presented isentropic data for compression up to 35 kbars (Ref. 33) utilizing the Sandia Laboratories Z-Machine. Both of these sets of data agree well with the impact shock data of Johnson *et al.*[34] For PDMS, Sachdev *et al.* measured isothermal compression of pure PDMS up to 4 kbars via a Nova Swiss pressure chamber coupled with optical observation of the volume change of the PDMS sample,[35] while Dattelbaum *et al.* performed shock compression of a low molecular weight (470 g/mol) pure PDMS sample.[36] Low-pressure dilatometry data have been reported for Sylgard® 184, a cross-linkable PDMS-based networked elastomer containing silica, by Dattelbaum *et al.*[1] Despite the differences in composition and molecular weight between pure PDMS and Sylgard®, excellent agreement in *PVT* behavior is observed between the two materials at low pressure. For higher pressure data, a Hugoniot shock compression curve for Sylgard® 184 has been generated from impedance-matched high explosive shock experiments performed at Los Alamos National Laboratories.[37] Additionally, Dattelbaum *et al.* employed a novel optical technique utilizing diamond anvil cells coupled with microscopic image analysis in order to provide data on the isothermal compression behavior of Sylgard® at high pressures.[1] That work represents the first measurement of isothermal compression of an amorphous polymer to pressures greater than 100 kbars. The high pressure behavior of Sylgard® has also been investigated using Brillouin scattering in a diamond anvil pressure cell by Stevens *et al.*[38] For PBD, Barlow[39] performed dilatometry of 1,4-*cis*-polybutadiene up to 3 kbars, while both Gupta and Gupta[40] and Millet *et al.*[41] performed shock Hugoniot experiments on hydroxyl-terminated polybutadiene (HTPB) using gas-gun plate impact experiments for cross-linked HTPB materials. In the case of Gupta and Gupta's data, little detail was given on the chemical nature of the HTPB employed, while Millet *et al.* performed experiments on both a proprietary HTPB formulation and a simple elastomeric HTPB composed of 12 wt % cross-linker. For the nonplasticized Estane®, Stevens *et al.*[38] provided both high pressure Brillouin scattering data and low-pressure dilatometry data. In addition, impedance-matched high explosive[37] and gas gun impact[34] shock Hugoniot data are available.

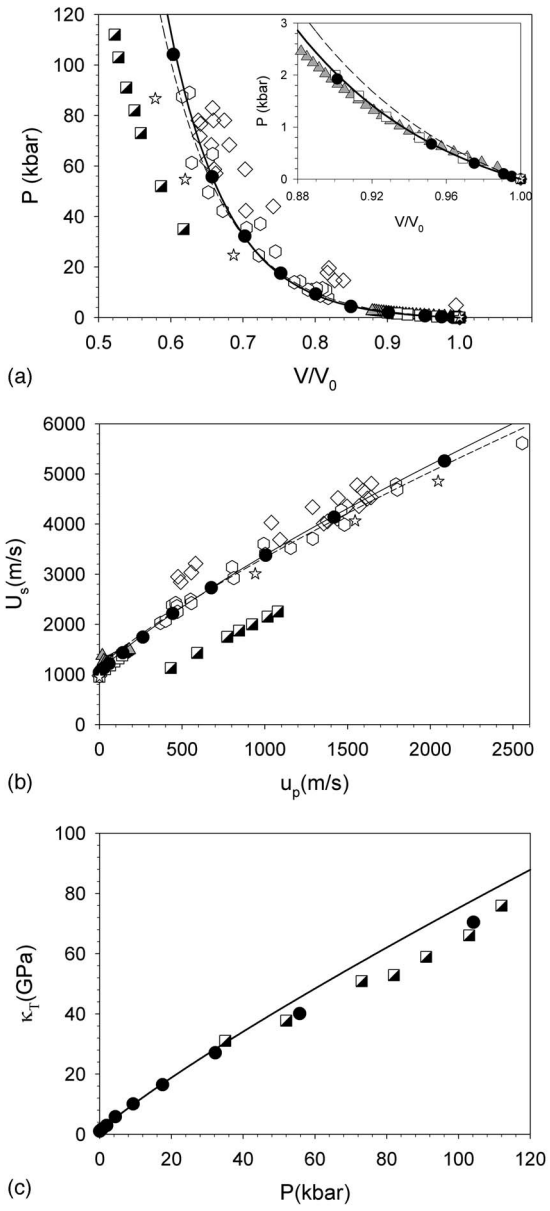

FIG. 2. (a) Comparison of experimental and simulation pressure vs compression data for Sylgard®/PDMS. Symbols represent data points from Dattelbaum *et al.* (Ref. 1) (diamonds), Marsh (Ref. 37) (hexagons), Sachdev *et al.* (Ref. 35) (triangles), Stevens *et al.* (Ref. 38) dilatometry (squares, empty) and Brillouin (squares, half-filled) experiments, and Dattelbaum *et al.* 470 g/mol (pure) PDMS (Ref. 36) (stars) and simulation (circles). The lines represent the fitted Tait EOS for both fitted (solid) and universal (dashed) values of C to the simulation data. The inset expands the low-pressure region of the data. (b) Comparison of the experimental and simulation $U_s - u_p$ data for Sylgard®/PDMS. All symbols and lines are as in (a). (c) Comparison of the experimental and simulation bulk modulus for Sylgard®/PDMS. All symbols and lines are as in (a).

B. Comparison between simulation and experiment

1. PDMS and Sylgard®

Figure 2(a) shows pressure as a function of compression for PDMS (simulation and experiment) and Sylgard® (experiment). Overall, the experimental data are mutually consistent and are in good agreement with the isothermal simulation results to high compression. The exception is the data for Sylgard® obtained from diamond anvil cell measurements. Discrepancies here could be due to stiffening of the polymer due to the N_2 hydrostatic medium penetrating the PDMS network in the optical measurements and uncertainties in determining the volume in the Brillouin measurements. We note that the Hugoniot data of Marsh[37] for Sylgard® are in good agreement with our simulation results for PDMS at all pressures. The relatively minor deviation from simulation observed for the 470 g/mol (pure) PDMS (Ref. 36) is expected due to the lower molecular weight of this material compared to the simulated PDMS (1571 g/mol). A study of the influence of molecular weight on isothermal compression behavior of PDMS has shown strong dependence on molecular weight for low molecular weights,[42] with lower molecular weight PDMS exhibiting greater relative compression at a given pressure than higher molecular weight PDMS. Dilatometry data for PDMS and Sylgard® are also in good agreement with each other and our simulation results at lower pressures. Figure 2(b) shows compression of PDMS and Sylgard® in the $U_s - u_p$ plane. Clear curvature, well known for PDMS, can be observed, particularly at lower pressures. Again, consistency between different sets of experimental data and between experimental data and simulation can be seen except for the data from Refs. 1 and 38.

Finally, Fig. 2(c) shows the bulk modulus for PDMS obtained from simulations compared with that obtained from Brillioun scattering measurements of sound speed. While the values obtained from fluctuations [Eq. (3)] are in good agreement with experiment over the range of experimental measurements, we believe this agreement to be fortuitous. At pressures above about 30 kbars, we find that fluctuations become unreliable due to their small magnitude (reflecting a large bulk modulus) in comparison with very slow "drift" in the average system volume. This slow continuous decrease in volume with simulation time adds to the apparent average instantaneous deviation of volume from the average volume [see Eq. (3)] and hence yields an artificially low bulk modulus. The drift in volume at higher pressures is a consequence of the pressure-induced melt-to-glass transition in the polymer, which is also observed in PBD and np-Estane. At lower pressures PDMS is a melt on simulation time scales, and hence we can sample equilibrium volume. At higher pressures, the polymer falls out of equilibrium on simulation time scales and exhibits slow volume relaxation from the quenched glassy state toward the equilibrium (liquid) density. We believe the bulk modulus obtained from the Tait EOS fit to the compression data [Eq. (4), see Sec. III C for discussion of the Tait EOS fit), which depends only on the volume at each pressure and not on the volume fluctuations, is a much better representation of the polymer bulk modulus in the glassy state. At lower pressures where fluctuations are reliable, good agreement between the bulk modulus from fluctuations and the EOS can be seen. At higher pressures, the bulk modulus from the EOS is greater than that seen experimentally for Sylgard® or from fluctuations. The source of the discrepancy between simulation (from EOS) and experiment for the bulk modulus at higher pressures is unclear.

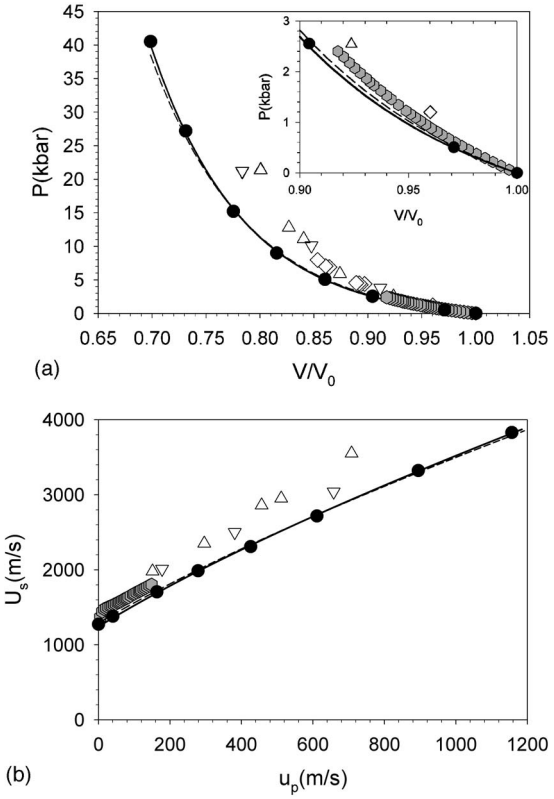

FIG. 3. (a) Comparison of experimental and simulation pressure vs compression data of HTPB/PBD systems. Symbols represent data points from Barlow (Ref. 39) (hexagons), Gupta and Gupta (Ref. 40) (diamonds), and Millet *et al.* (Ref. 41) HTPB1 (triangles, up) and HTPB2 (triangles, down), and simulation (circles). The lines represent the fitted Tait EOS for both fitted (solid) and universal (dashed) values of C to the simulation data. The inset expands the low-pressure region of the data. (b) Comparison of the experimental and simulation U_s-u_p data for HTPB/PBD systems. All symbols and lines are as in (a).

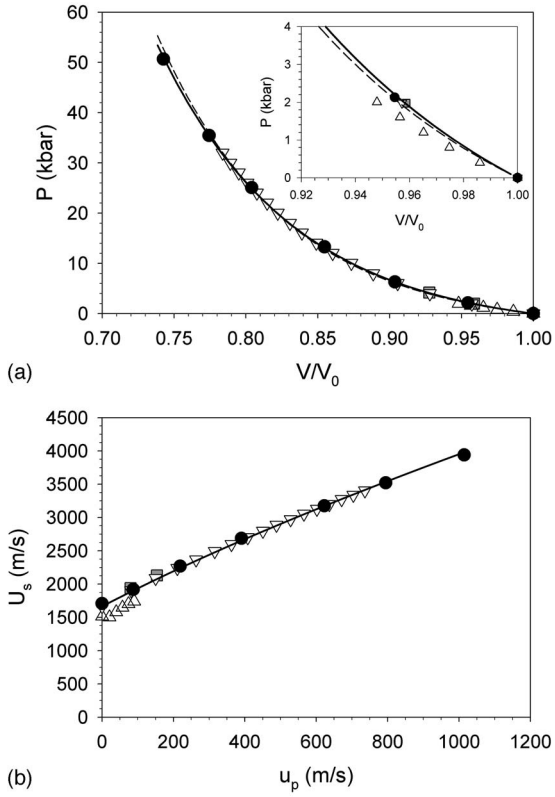

FIG. 4. (a) Comparison of experimental and simulation pressure vs compression data for np-Estane. Symbols represent data points from Johnson *et al.* (Ref. 34) (squares), Gustavsen *et al.* (Ref. 33) dilatometry (triangles, up) and isentropic Z-Machine (triangles, down), and simulation (circles). The lines represent the fitted Tait EOS for both fitted (solid) and universal (dashed) values of C. The inset expands the low-pressure region of the data. (b) Comparison of the experimental and simulation U_s-u_p data for np-Estane. All symbols and lines are as in (a).

2. PBD and HTPB

Figure 3(a) shows pressure as a function of compression for PBD and HTPB from simulation and experiment, while Fig. 3(b) shows compression data in the U_s-u_p plane. Our 1,4-PBD is significantly less stiff than the HTPB materials for which experimental data are available. HTPB, as discussed above, while largely PBD, often includes additives and is highly cross-linked. The *cis*-1,4-PBD utilized in the dilatometry study of Barlow[39] is in much better agreement with our PBD results. The *cis*-1,4-PBD is likely of much higher molecular weight than our simulation material and is of a different microstructure (all *cis* units versus the random copolymer *cis*, *trans*, and *vinyl* units we are simulating), which may account in part for the discrepancy observed between simulation and experiment.

3. np-Estane

Figure 4(a) shows pressure as a function of compression for np-Estane from simulation and experiment, while Fig. 4(b) shows compression data in the U_s-u_p plane. Agreement between simulation and experiment is excellent except for the low-pressure dilatometry measurements. Conversion of $P(V)$ from dilatometry to the U_s-u_p plane appears to indicate some inconsistency with these data.

4. Model Estane®

Figure 5(a) shows pressure as a function of compression for our model Estane® polymer from simulation and compares them with experimental results for Estane®. While the simulation is in reasonable agreement with the Hugoniot-based shock experiments as well as the dilatometry measurements, there is a notable discrepancy between the Brillouin scattering based predictions and the remainder of the data and simulation results. As discussed above with regard to the PDMS system, this difference may be attributable to the difficulty in accurately determining the volume when utilizing the Brillouin scattering technique. The same discrepancy is also visible in the U_s-u_p plane comparison of Fig. 5(b).

C. Tait EOS and universal behavior

The fits of the Tait EOS to simulation compression data using the universal C parameter ($C=0.089\,36$) as well as the best fit obtained by allowing C to vary are shown in Figs. 2(a), 3(a), 4(a), and 5(a) for PDMS, PBD, np-Estane, and model Estane® respectively. Tait EOS parameters are summarized in Table II including the zero-pressure bulk modulus κ_0 from Eq. (5) and from fluctuations [Eq. (3)]. We note that κ_0 from fluctuations and from the best-fit Tait EOS to the simulation data are in remarkably good agreement for all polymers. Utilizing κ_0 from fluctuations as a normalizing

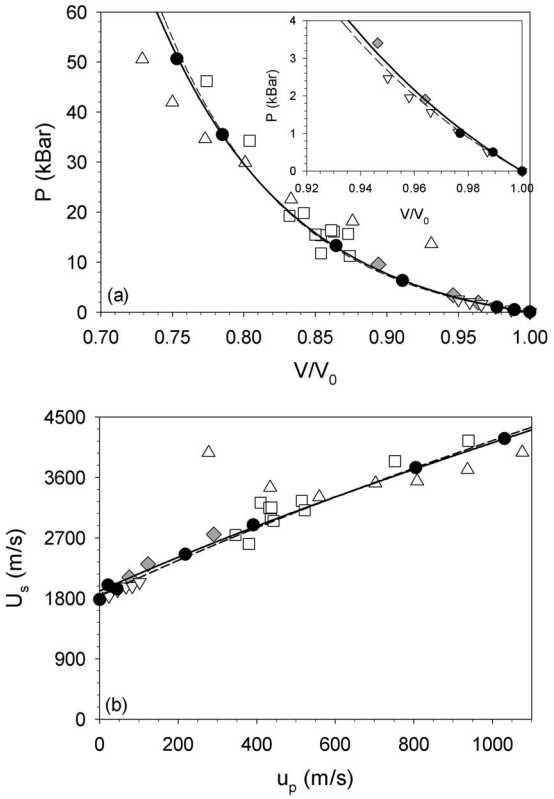

FIG. 5. (a) Comparison of experimental and simulation pressure vs. compression data for Estane®. Symbols represent data points from Johnson *et al.* (Ref. 34) (diamonds), Stevens *et al.* (Ref. 38) dilatometry (triangles down) and Brillouin scattering (triangles up), and Marsh (Ref. 37) (squares). The lines represent the as fit Tait EOS for both fitted (solid) and universal (dashed) values of *C*. The inset expands the low-pressure region of the data. (b) Comparison of the experimental and simulation U_s-u_p data for Estane®. All symbols and lines are as in (a).

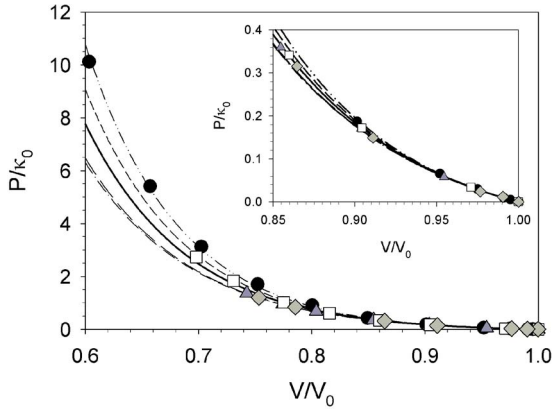

FIG. 6. (Color online) Comparison of the normalized pressure (P/κ_0) as a function of compression for the simulated PDMS (circles), PBD (squares), np-Estane (triangles), and model Estane® (diamonds) systems. The lines are normalized Tait equations of state [Eq. (6)] as fit for individual polymers (dash-dot-dot, short dashes, long dashes, dash-dot for PDMS, PBD, np-Estane, and model Estane® respectively) as well as utilizing the universal *C* value of 0.089 36 (solid line).

parameter, we have plotted normalized pressure (P/κ_0) as a function of compression for each polymer in Fig. 6. Also shown is normalized pressure versus compression from the best-fit Tait EOS [Eq. (6)] for each polymer as well as the universal compression behavior predicted by the Tait EOS [Eq. (6) with $C=0.089\,36$]. Figure 6 reveals that the compression of all three polymers is reasonably described by the Tait universal compression curve, while relatively minor adjustments in the *C* parameter results in an excellent description of compression for all three polymers.

Using the Tait EOS parameters given in Table II as determined from fits to simulation data in the *P-V* plane, we have utilized Eqs. (9) and (10) to predict compression in the U_s-u_p plane, as shown in Figs. 2(b), 3(b), 4(b), and 5(b) for PDMS, PBD, np-Estane, and model Estane®, respectively. In the normalized U_s-u_p plane (U_s/C_o versus u_p/C_o), the Tait EOS again predicts universal behavior using $C=0.089\,36$ [Eqs. (11) and (12)], as shown in Fig. 7. As with compression, the universal curve provides a reasonable description of the compression of all four polymers, although the description is improved when the polymer-dependent *C* parameter given in Table II is employed, as shown in Fig. 7. Note that all four polymers exhibit curvature (nonlinear behavior) in the U_s-u_p plane that is well captured by the Tait EOS. Finally, Fig. 8 shows the normalized pressure-dependent bulk modulus κ_T/κ_0 as a function of normalized pressure from the best-fit Tait EOS, deemed to be our best estimate of the bulk modulus, for each polymer [Eq. (7)] as well as the universal Tait EOS prediction [Eq. (7) with $C=0.089\,36$]. The univer-

TABLE II. The Tait EOS parameters for the simulated systems. Shaded cells represent the "best-fit" values for the Tait EOS wherein both the *C* and *B* parameters were fitted. The nonshaded cells represent the fit produced utilizing the universal *C* constant of 0.089 36.

	C	*B* (GPa)	κ_0 (GPa) Tait EOS [Eq. (5)]	κ_0 [GPa] fluctuations [Eq. (3)]
Poly (DimethylSiloxane)	0.081 83	0.085 66	1.047	1.029
	0.089 36	0.114 25	1.279	
Poly (Butadience)	0.085 59	0.121 04	1.414	1.485
	0.089 36	0.136 15	1.524	
Nitroplasticized Estane	0.094 25	0.355 96	3.777	3.700
	0.089 36	0.313 22	3.505	
Model Estane®	0.094 90	0.411 46	4.334	4.216
	0.089 36	0.356 89	3.994	

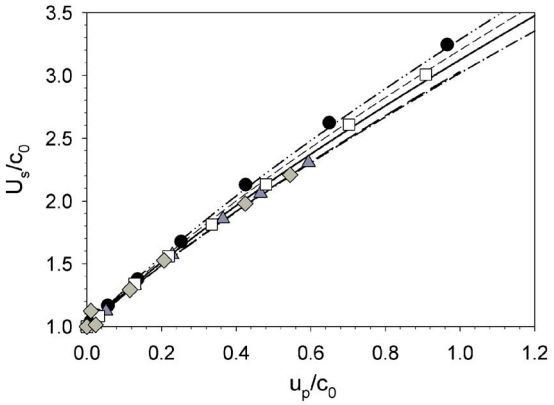

FIG. 7. (Color online) Comparison of the normalized U_s-u_p curves (U_s/c_0 vs u_p/c_0) for the as fit from the simulated PDMS (circles), PBD (squares), np-Estane (triangles), and model Estane® (diamonds) systems. The lines are normalized Tait fits [Eqs. (11) and (12)] for U_s/c_0 vs u_p/c_0 utilizing the C parameter from PDMS (dash-dot-dot), PBD (short dashes), np-Estane (long dashes), model Estane® (dash-dot), and the universal C parameter of 0.089 36 (solid).

sal Tait EOS provides a reasonable prediction of the normalized bulk modulus of all four polymers.

D. Free volume

Figures 2(a), 3(a), 4(a), and 5(a), as well as Fig. 6, reveal that compression of PDMS, PBD, np-Estane, and model Estane® to high pressures is well described by the Tait EOS. In order to apply the Tait EOS to a polymer of interest, it is necessary to know only the zero-pressure bulk modulus κ_0 if universal behavior is assumed (a polymer-independent value of C). For the polymers studied here, κ_0 varies widely (around 1 GPa for PDMS to slightly above 4 GPa for the model Estane system), as given in Table II. A more accurate prediction of *PVT* behavior is obtained if knowledge of the

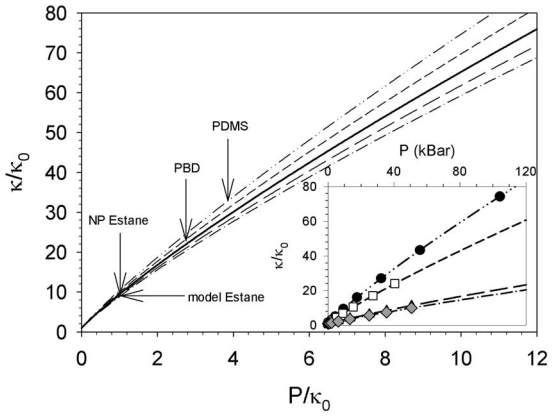

FIG. 8. The Tait EOS predictions [Eq. (7)] for the normalized, pressure-dependent bulk modulus (κ_T/κ_0) vs normalized pressure (P/κ_0) for fits utilizing the C parameter derived from PDMS (dash-dot-dot), PBD (short dashes), np-Estane (long dashes), model Estane® (dash-dot), and the universal C parameter of 0.089 36 (solid). The arrows representing the different polymers are located at a constant pressure of 40 kbars, and highlight the different rates of growth of the normalized modulus at constant pressure. The inset shows the growth in the normalized, pressure-dependent bulk modulus vs gauge pressure, where the lines have the same meaning as above and the symbols denote the simulated pressures for PDMS (circles), PBD (squares), np-Estane (triangles), and model Estane® (diamonds).

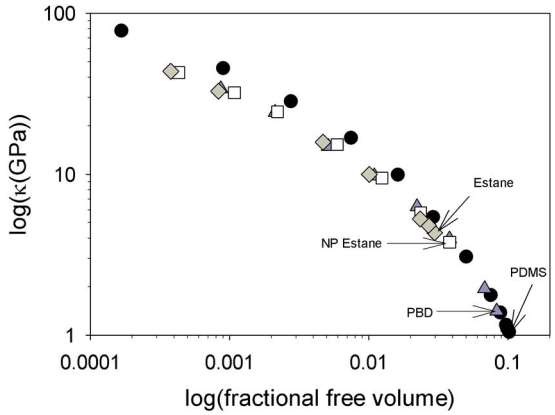

FIG. 9. (Color online) Log of the pressure-dependent bulk modulus κ_T vs the logarithm of the fractional free volume f_{fv} for PDMS (circles), PBD (squares), np-Estane (triangles), and model Estane® (diamonds). The arrows denote the atmospheric (κ_0) value of the bulk modulus.

value of the C parameter most appropriate for the polymer of interest can be obtained.

PDMS has high fractional free volume ($f_{fv}=V_f/V$, where V_f is free volume) and low zero-pressure bulk modulus compared to most polymers. Furthermore, the relative increase in bulk modulus with pressure, κ_T/κ_0, is particularly large for PDMS at a given pressure compared to most other polymers. This can be clearly seen in the inset of Fig. 8 where the relative increase in bulk modulus is shown as a function of pressure for the four polymers. In terms of the Tait EOS [Eq. (7)], this behavior can be understood as being due to the fact that the normalized pressure (P/κ_0) is greater at a given pressure for a polymer with a low κ_0 compared to polymers with higher κ_0. For example, P/κ_0 corresponding to 40 kbars is shown for PDMS, PBD, and np-Estane in Fig. 8 on the universal κ_T/κ_0 curve from the Tait EOS.

Physically, the low-pressure "crush-up" of PDMS, i.e., the rapid increase in relative modulus at low pressures, has been interpreted in terms of rapid loss of the initially high fractional free volume with increasing pressure.[1] In order to explore the relationship between bulk modulus and free volume, we have probed free volume in each system at multiple pressures, as described in Sec. II C, and have plotted κ_T [from the best-fit Tait EOS, Eq. (4)] as a function of f_{fv} for PDMS, PBD, np-Estane, and model Estane®, as shown in Fig. 9. The ambient pressure free volume/bulk modulus is indicated for each polymer. A strong correlation between bulk modulus and fractional free volume independent of the particular polymer can be observed up to high pressures/low fractional free volume. Such a correlation allows for the estimation of κ_0, needed for application of the Tait EOS, for a polymer of interest, from knowledge of the fractional free volume for that polymer at ambient pressure. It appears that it may also be possible to obtain a reasonable estimate of $\kappa_T(P)$ at a pressure of interest given knowledge of the fractional free volume for a polymer at pressure P. Determination of f_{fv} as described in Sec. II C requires fewer computational resources than accurate determination of κ_0 from fluctuations or simulations at multiple pressures required to fit an EOS. We also note that at ambient pressure the np-Estane has slightly greater free volume than the pure model

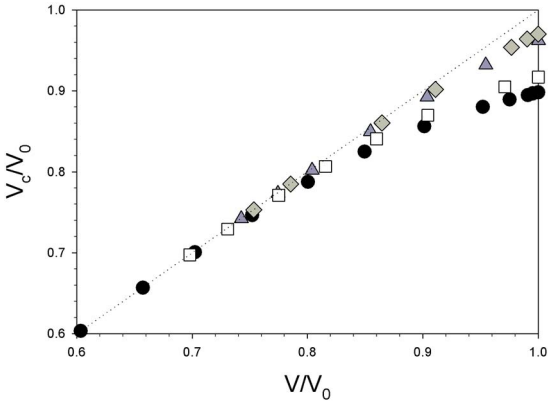

FIG. 10. (Color online) The core volume $(V-V_f)$ normalized by the zero-pressure volume V_0 as a function of compression ratio for PDMS (circles), PBD (squares), np-Estane (triangles), and model Estane® (diamonds). The dashed line represents the asymptotic limit wherein compression has removed all the free volume from the system and the core volume ratio is equivalent to the overall compression ratio.

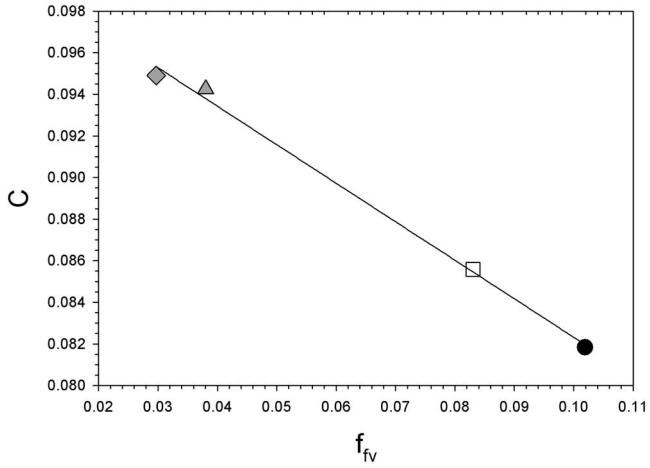

FIG. 11. The best-fit value of C for the Tait EOS vs the atmospheric pressure free volume percentage for PDMS (circle), PBD (square), np-Estane (triangle), and model Estane® (diamond). The line is a linear fit with equation $C=0.1008-0.1852f_{fv}$.

Estane®, consistent with the presence of the low molecular weight plasticizer in the former. The greater free volume of the np-Estane compared to the nonplasticized polymer leads to a slightly decreased κ_0, as can be seen in Table II and Fig. 9.

Examining f_{fv} as a function of pressure also provides insight into the greater crush-up observed in PDMS compared to PBD and the Estane-based systems. Figure 10 shows the core volume $(V-V_f)$ normalized by the zero-pressure volume V_0 as a function of compression ratio for the four polymers. When the slope of this function approaches unity, as observed at higher compression, nearly all volume change with increasing pressure comes from decreasing core volume. Strong deviation from a unity slope indicates that decreasing free volume is contributing significantly to compression. Figure 10 reveals that at low pressure, decreasing free volume is relatively unimportant for compression of the Estane-based systems, which are relatively stiff at ambient pressure, have relatively little free volume, and have less increase in normalized modulus with pressure. In contrast, for PDMS, which has greater free volume and is relatively compliant at ambient pressure, initial compression comes at the expense of free volume and results in significant stiffening of the polymer at lower pressures, as can be observed in the inset of Fig. 8.

Finally, Fig. 11 shows the best-fit Tait EOS C parameter as a function of f_{fv} at atmospheric pressure. The relationship can be well approximated by a linear fit, allowing for straightforward estimate of the C given knowledge of fractional free volume at ambient pressure. This fit predicts a monotonic shift of the C parameter to higher values with decreasing fractional free volume, with the universal value $(C=0.089\,36)$ falling roughly in the middle of the investigated polymers.

IV. CONCLUSIONS

A MD simulation study of the *PVT* behavior up to 100 kbars of four polymers important in energetic materials and explosives applications (PDMS, PBD, np-Estane, and a pure model Estane®) has been conducted. Compression, U_s-u_p, and $\kappa_T(P)$ have been compared with experimental data on the same and related polymers, revealing that MD simulations utilizing validated potentials can be used to accurately predict the *PVT* behavior of polymers to high pressures. We find that all three polymers are well described by the Tait EOS and can be described reasonably well by universal *PVT* behavior despite their very different ambient pressure stiffness (κ_0). Hence, knowledge of κ_0 alone, at least for the four polymers investigated, allows for reasonably accurate prediction of *PVT* behavior to high pressures. More accurate predictions are possible by allowing the Tait EOS C parameter to depend on the polymer. Both κ_0 and the Tait EOS C parameter were found to correlate with fractional free volume, allowing for accurate estimate of *PVT* behavior to high pressures based only on the knowledge of ambient pressure fractional free volume, which can be readily obtained from simulations.

ACKNOWLEDGMENTS

J.B.H., D.B., and G.D.S. gratefully acknowledge the financial support of the University of Utah Center for the Simulation of Accidental Fires and Explosions (C-SAFE), funded by the Department of Energy, Lawrence Livermore National Laboratory, under Subcontract No. B341493, as well as support from the Department of Energy, Los Alamos National Laboratory, under Contract No. LANL-0591300104. An allocation of computer time from the Center for High Performance Computing at the University of Utah is gratefully acknowledged. O.B. acknowledges support from the Air Force Office of Scientific Research (Contract No. FA8651-08-M-0125).

[1] D. M. Dattelbaum, J. D. Jensen, A. M. Schwendt, E. M. Kober, M. W. Lewis, and R. Menikoff, J. Chem. Phys. **122**, 144903 (2005).
[2] R. H. Boyd and G. D. Smith, *Polymer Dynamics and Relaxation* (Cambridge, New York, 2007).
[3] T. D. Sewell, R. Menikoff, D. Bedrov, and G. D. Smith, J. Chem. Phys. **119**, 7417 (2003).
[4] O. Borodin, G. D. Smith, T. D. Sewell, and D. Bedrov, J. Phys. Chem. B

112, 734 (2008).
[5] J. S. Smith, O. Borodin, G. D. Smith, and E. M. Kober, J. Polym. Sci., Part B: Polym. Phys. **45**, 1599 (2007).
[6] See EPAPS Document No. E-JCPSA6-130-039907 for a full description of the PDMS force field form and parameters employed. For more information on EPAPS, see http://www.aip.org/pubservs/epaps.html.
[7] G. D. Smith, W. Paul, M. Monkenbusch, L. Willner, D. Richter, X. H. Qiu, and M. D. Ediger, Macromolecules **32**, 8857 (1999).
[8] O. Byutner and G. D. Smith, Macromolecules **34**, 134 (2001).
[9] G. D. Smith, O. Borodin, D. Bedrov, W. Paul, X. H. Qiu, and M. D. Ediger, Macromolecules **34**, 5192 (2001).
[10] O. Byutner and G. D. Smith, Macromolecules **35**, 3769 (2002).
[11] G. D. Smith, O. Borodin, and W. Paul, J. Chem. Phys. **117**, 10350 (2002).
[12] G. D. Smith, D. Bedrov, and W. Paul, J. Chem. Phys. **121**, 4961 (2004).
[13] D. Bedrov, G. D. Smith, and W. Paul, Phys. Rev. E **70**, 011804 (2004).
[14] W. Paul, D. Bedrov, and G. D. Smith, Phys. Rev. E **74**, 021501 (2006).
[15] G. D. Smith and D. Bedrov, J. Non-Cryst. Solids **352**, 4690 (2006).
[16] G. D. Smith and D. Bedrov, J. Polym. Sci., Part B: Polym. Phys. **45**, 627 (2007).
[17] H. Davande, D. Bedrov, and G. D. Smith, J. Energ. Mater. **26**, 1 (2008).
[18] G. D. Smith, D. Bedrov, O. G. Byutner, O. Borodin, C. Ayyagari, and T. D. Sewell, J. Phys. Chem. A **107**, 7552 (2003).
[19] H. Davande, O. Borodin, G. D. Smith, and T. D. Sewell, J. Energ. Mater. **23**, 205 (2005).
[20] http://www.eng.utah.edu/~gdsmith/lucretius.html.
[21] S. Nosé, J. Chem. Phys. **81**, 511 (1984).
[22] W. G. Hoover, Phys. Rev. A **31**, 1695 (1985).
[23] H. C. Anderson, J. Chem. Phys. **72**, 2384 (1980).
[24] J. Ryckaert, G. Ciccotti, and H. J. C. Berendsen, J. Comput. Phys. **23**, 327 (1977).
[25] T. Darden, D. York, and L. Pedersen, J. Chem. Phys. **98**, 10089 (1993).
[26] G. J. Martyna, M. E. Tuckerman, and D. J. Tobias, Mol. Phys. **87**, 1117 (1996).
[27] V. S. Nanda and R. Simha, J. Chem. Phys. **41**, 1884 (1964).
[28] R. R. Matheson, Jr., J. Phys. Chem. **91**, 6062 (1987).
[29] J. M. Smith, H. C. Van Ness, and M. M. Abbott, *Introduction to Chemical Engineering Thermodynamics* (McGraw-Hill, New York, 2001).
[30] M. P. Allen and T. J. Tildesley, *Computer Simulations of Liquids* (Oxford University Press, Oxford, 1987).
[31] M. L. Wilkins, *Computer Simulation of Dynamic Phenomena* (Springer, Berlin, 1999).
[32] B. Olinger and P. M. Halleck, J. Chem. Phys. **62**, 94 (1975).
[33] R. L. Gustavsen, D. M. Dattelbaum, E. B. Orler, D. E. Hooks, R. R. Alcon, S. A. Sheffield, C. E. Hall, and M. R. Baer, in *Shock Compression of Condensed Matter*, edited by M. D. Furnish, M. Elert, T. P. Russell, and C. T. White (Springer, Berlin, 2005), p. 149.
[34] N. Johnson, J. J. Dick, and R. S. Hixson, J. Appl. Phys. **84**, 2520 (1998).
[35] V. K. Sachdev, Y. Yahsi, and R. K. Jain, J. Polym. Sci., Part B: Polym. Phys. **36**, 841 (1998).
[36] D. M. Dattelbaum (unpublished data).
[37] *LASL Shock Hugoniot Data*, edited by S. P. Marsh (University of California Press, Berkeley, 1980).
[38] L. L. Stevens, E. B. Orler, D. M. Dattelbaum, M. Ahart, and R. J. Hemley, J. Chem. Phys. **127**, 104906 (2007).
[39] J. W. Barlow, Polym. Eng. Sci. **18**, 238 (1978).
[40] S. C. Gupta and Y. M. Gupta, High Press. Res. **19**, 785 (1992).
[41] J. C. F. Millet, N. K. Bourne, and J. Akhavan, J. Appl. Phys. **95**, 4722 (2004).
[42] R. N. Lichtenthaler, D. D. Liu, and J. M. Prausnitz, Macromolecules **11**, 192 (1978).